Nuclear Instruments and Methods in Physics Research A 1080 (2025) 170698

Contents lists available at ScienceDirect

Nuclear Inst. and Methods in Physics Research, A

journal homepage: www.elsevier.com/locate/nima

Characterization of a 4H–SiC neutron detector in the neutron field of an accelerator-based BNCT facility

Qiuying Li [a], Jinlin Song [a], Zhimeng Hu [a,b,*], Wenbo Liu [a], Fule Li [a], Mingcai Zhong [a], Pin Gong [a,b], Wei Jiang [c], Kang Sun [c], Giuseppe Gorini [d], Gabriele Croci [d], Meng Li [e], Youqun Lai [f], Xiaobin Tang [a,b]

[a] Department of Nuclear Science & Technology, Nanjing University of Aeronautics and Astronautics, Nanjing, 211106, China
[b] Key Laboratory of Advanced Nuclear Technology and Radiation Protection, Ministry of Industry and Information Technology, Nanjing University of Aeronautics and Astronautics, Nanjing, 211106, China
[c] Spallation Neutron Source Science Center, Dongguan, 523803, China
[d] Department of Physics, University of Milan-Bicocca, Milan, 20126, Italy
[e] Neuboron Therapy System Ltd., Xiamen, 361000, China
[f] BNCT Center, Xiamen Humanity Hospital, Xiamen, 361006, China

ARTICLE INFO

Keywords:
Neutron detectors
Beam monitor
BNCT
SiC detector
Charge collection efficiency

ABSTRACT

4H–SiC features excellent properties such as wide bandgap and fast carrier drift velocity, making it a good semiconductor candidate for developing neutron detectors with hard resistance, fast response, high charge collection efficiency and excellent thermal stability. However, to date there remains a scarcity of comprehensive studies on the performance of 4H–SiC based neutron detectors working in the neutron field of an accelerator-based Boron Neutron Capture Therapy (AB-BNCT) facility. In our work, a ^{6}LiF thermal neutron convertor was coated with the 4H–SiC detector to enhance the sensitivity to thermal neutrons by employing the ^{6}Li (n, α) T nuclear reaction. The 4H–SiC detector yields a pulse height spectrum which has a clear Triton peak isolated from other structures, demonstrating its good background rejection ability. Good performance is also revealed by the excellent linear relationship between count rates of the detector and beam intensities of the AB-BNCT accelerator, consistency between the detector and a standard neutron yield monitor of the AB-BNCT in their time-dependent count rates, and long-time stability in both the count rate and the pulse height spectrum shape. Based on the TCAD simulations, the 4H–SiC detectors were found to have high resistance to neutron radiation in BNCT, with charge collection efficiencies exceeding 95 % even at neutron fluences up to 10^{16} cm^{-2}. Due to the compact volume, the 4H–SiC detectors have the potential to develop high-performance neutron fluence and spectrum monitoring instruments for AB-BNCT facilities.

1. Introduction

High energy neutrons in an accelerator-based BNCT (AB-BNCT) are generated by bombarding targets with charged particles provided by an accelerator. These neutrons are then moderated by a beam shaping assembly (BSA) to thermal or epithermal energies for cancer treatment [1–3]. AB-BNCT eliminates reliance on nuclear reactors, thereby bypassing their regulatory constraints and enabling scalable deployment in cancer therapy [4]. The BSA is generally designed using the Monte Carlo simulations. However, the predicted neutron spectra and spatial distributions of neutron flux at the beam exit of an AB-BNCT might deviate to some extent from the real values due to the difficulties in adequately describing the geometry dimensions, material contents and mass densities of components of the BSA. The large size of the BSA makes the predictions of neutron flux and spectrum with high reliability even harder. Additionally, the presence of instabilities in the charged particle beam caused by internal malfunctions and space charge effects in the accelerator [5,6], as well as long-term irradiation-induced degradation and blistering of targets [7,8] would lead to changes in the therapeutic neutron beams and cause bias in the neutron dose delivered to the patient. Therefore, experimental verification of the calculated neutron fluence distribution and energy spectrum at the beam exit, in

* Corresponding author. Department of Nuclear Science & Technology, Nanjing University of Aeronautics and Astronautics, Nanjing, 211106, China..
E-mail address: huzhm21@nuaa.edu.cn (Z. Hu).

https://doi.org/10.1016/j.nima.2025.170698
Received 3 April 2025; Received in revised form 20 May 2025; Accepted 24 May 2025
Available online 24 May 2025

conjunction with online monitoring of neutron beams are crucial to guarantee the efficacy of BNCT treatment.

The 4H–SiC material features a wide bandgap (3.27 eV) and a high atomic displacement threshold energy (21 eV for carbon, 35 eV for silicon), which endows the detector with excellent signal-to-noise ratio under low leakage current conditions and outstanding radiation resistance [9–11], and exhibits excellent performance in intense neutron field measurements. For instance, in a D-T fusion neutron irradiation experiment, the charge collection efficiency (CCE) decreased by only 7 % when the neutron fluence reached 1.31×10^{14} cm^{-2} [12]. A neutron flux monitor based on the 4H–SiC detector has a good linear response over a neutron yield range of 10^{12}–10^{15} per discharge in the EAST tokamak [13]. Additionally, the maximum breakdown electric field of 4H–SiC is eight times that of silicon, allowing for higher drift velocity and more efficient charge collection under higher bias voltages. Studies have demonstrated that a 4H–SiC detector with the sensitive region thickness of 50 μm had a current signal width of <2 ns [14].

Given the favorable characteristics of 4H–SiC detectors, they are well-suited for developing high-performance neutron fluence and spectrum monitoring instruments for AB-BNCT facilities. The typical neutron field of an AB-BNCT facility has a large-area with a diameter of several tens of centimeters and a high neutron flux of approximately 10^9 cm^{-2} s^{-1} at the beam exit [15]. To enable neutron fluence and spectrum monitoring in AB-BNCT, the key challenge lies in fabricating thermal neutron counters with superior performance using 4H–SiC detectors. The electrode surface of a 4H–SiC detector can be coated with thermal neutron-sensitive materials such as ^{6}LiF or B_4C to make thermal neutron counters, which can count thermal neutrons by recording the charged particles produced in neutron convertors via neutron capture reaction [16]. Furthermore, the flux monitoring of epithermal and fast neutrons in an AB-BNCT can be realized by surrounding the 4H–SiC detector-based thermal neutron counter with a well-designed moderator. 4H–SiC belongs to semiconductor material and therefore can be fabricated into a large area 2-D array of pixelated detectors working as neutron flux monitors with good spatial resolution [17,18]. A neutron spectrometer with high energy resolution can be developed by embedding several 4H–SiC detector-based thermal neutron counters at different depths within a neutron moderator for neutron spectrum characterization and neutron field validation prior to each AB-BNCT treatment [19]. In addition, despite the excellent radiation resistance of 4H–SiC, prolonged exposure to intense neutron fields induces lattice damage that would trigger polarization effect, thereby degrading pulse height spectra and possibly affecting the count rate accuracy of the detector [14,20].

To address the above issues, the performance of a 4H–SiC detector-based thermal neutron counter is investigated when working in an AB-BNCT neutron field. Firstly, measurements with an α particle source for optimizing operation parameters were presented in Section 2. Subsequently, response linearity tests are conducted at different beam intensities of an AB-BNCT facility, followed by irradiation stability tests under continuous operation at the maximum beam intensity. The impact of AB-BNCT neutron irradiation on the output performance of the 4H–SiC detector is analyzed by using the TCAD simulations. Furthermore, comparing with the standard neutron yield monitor (a BF_3 gas thermal neutron counter) currently used at the AB-BNCT facility in Xiamen Humanity BNCT Center, the stability of the 4H–SiC detector is further verified.

2. Measurement with an α source

Fig. 1 shows the 2D schematic diagram of the 4H–SiC detector used in the experiment. The detector was based on a PIN diode with a sensitive area of 1 cm^2. A 30 μm epitaxial layer (doping = 2×10^{14} cm^{-3}), used as the sensitive volume, is grown on a 360 μm n-type 4H–SiC substrate (doping = 5×10^{18} cm^{-3}). A 0.5 μm thick p + region (doping = 1×10^{19} cm^{-3}) formed on the n-type 4H–SiC epitaxial layer. Ohmic contacts are formed using Ti/Ni metal stack for both the bottom substrate and the top p + region electrode. The detector is housed in a rectangular box made from aluminum with a circular hole facing the sensitive area. Deposited on the inner face of the lid for covering the hole is a 5 μm thick and 7 mm diameter's LiF thermal neutron convertor with an enrichment of ^{6}Li to 90 %. The air gap between the convertor and detector contact is 2 mm. Thermal neutrons can react with ^{6}Li in the convertor by emitting in opposite direction 2.73 MeV tritons and 2.05 MeV α particles which can be recorded by the 4H–SiC detector [21].

A 5.48 MeV ^{241}Am standard α source at the China Spallation Neutron Source was used to determine the suitable bias voltage of the 4H–SiC detector. The detector and α-source were located in a metal vacuum chamber, where a high vacuum of 0.1 Pa was maintained using a molecular pump. A charge amplifier CIVIDEC Cx-L was connected to the detector via an adapter in the vacuum chamber wall. The output signals from the amplifier were recorded by a CAEN DT5751 waveform digitizer (10 bit, 1 GS/s).

Bias voltages of 50, 100, 150, 200, 250, and 300 V were applied, and approximately 30,000 particles were collected over 120 s at a count rate of about 250 cps. The peak positions and energy resolutions at these bias voltages are shown in Fig. 2(a). The peak positions are stable when increasing the bias voltages between 50 V and 300 V. Peak position corresponds to the collected charges that are deposited by incidents particles in the sensitive volume. The 5.48 MeV α particles have a range of 18.3 μm in the SiC material. As shown in Fig. 3, when the voltages are below 100 V, the sensitive region thickness is narrower than the range of incident α particles and not all deposited charges can be collected by the detector, which could explain the slight increase of peak positions when increasing voltages from 50 V to 100 V. The full width at half maximum (FWHM) decreases rapidly when increasing the voltages to 150 V and becomes stable, reflecting that electric field strength plays a critical role in enhancing the energy resolution [22]. For example, at 100 V even though the sensitive region is thicker than the range of incident α particles, at the end of range the electric field strength is insufficient to

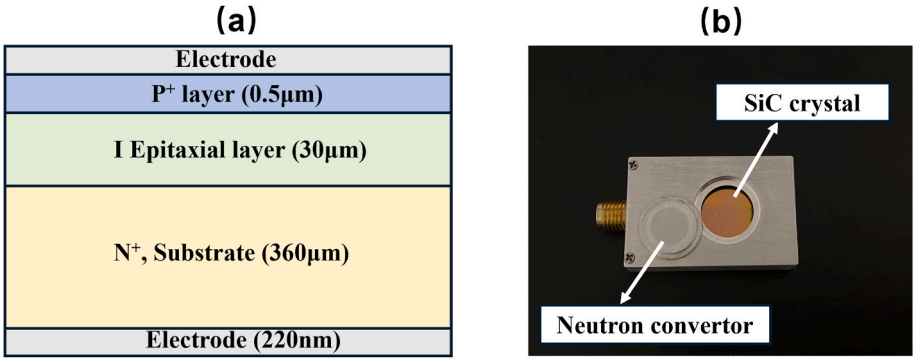

Fig. 1. (a) Schematic of the 2D structure of the 4H–SiC detector; (b) physical view of the 4H–SiC detector.

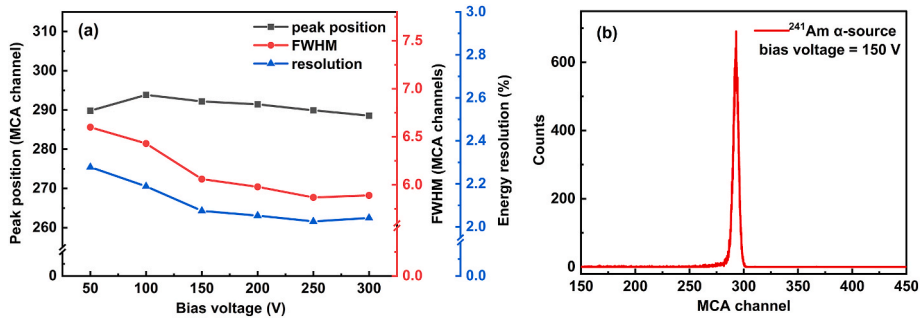

Fig. 2. (a) The peak position, FWHM, and energy resolution of the 4H–SiC detector measured at different bias voltages; (b) a pulse height spectrum of the 4H–SiC detector irradiated with a ^{241}Am α-source at the bias voltage of 150 V.

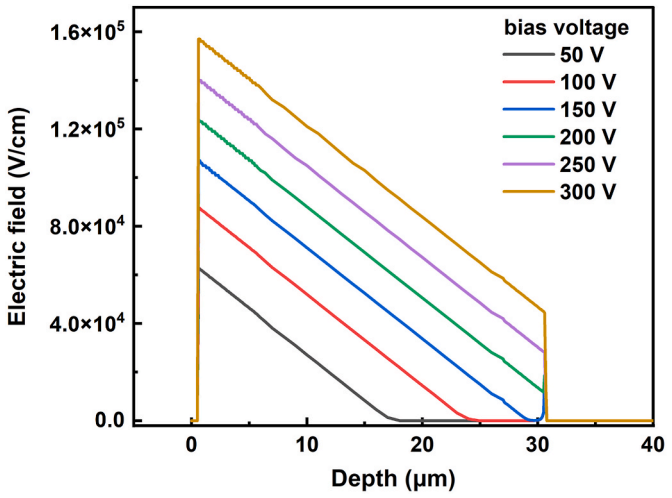

Fig. 3. Electric field distribution in the epitaxial layer of the 4H–SiC detector at different bias voltages.

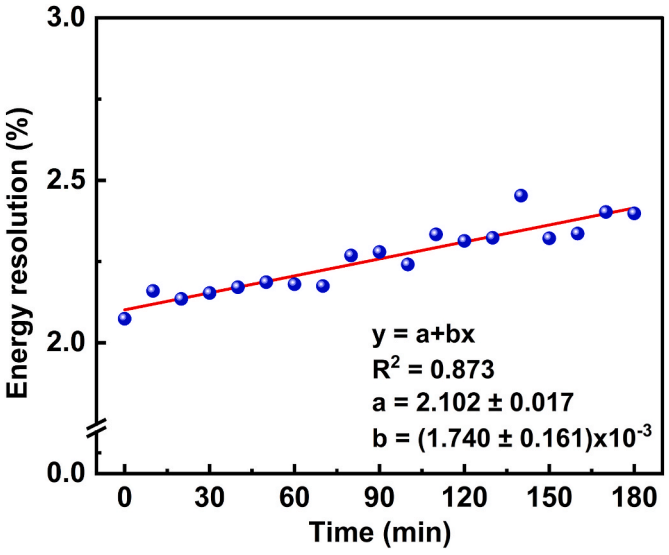

Fig. 4. Variation of the energy resolution with time for about 3 h. Error bars are smaller than the symbol size (<0.01 %) and thus not visible.

efficiently collect the deposited charges concentrated at the Bragg peak where the highest density of ionized charges accumulates. We can also find that too high electric field strength will lead to the FWHM increase and peak position reduce because of the leakage current increase, resulting in energy resolution deterioration. The combined effects analyzed above makes the 4H–SiC detector have the best energy resolution at ~150 V.

At the optimal bias voltage of 150 V, the pulse height spectrum (PHS) is depicted in Fig. 2(b) yielding the energy resolution of 2.05 %. The energy resolution uncertainties are less than 0.1 % and obtained from the Gaussian fitting process. The total counts under the PHS peaks are about 30000. This resolution is worse than the best result of 0.29 % for a 4H–SiC detector claimed in reference [23] and close to the best result achieved with a single crystal diamond detector (1.80 %) under the same experimental setup[24], demonstrating the good energy resolving capability of the 4H–SiC detector to charged particles.

Owing to the constraints of crystal fabrication processes, detectors inherently exhibit a certain degree of defects, and prolonged irradiation may lead to severe polarization effects [25,26], thereby deteriorating the energy resolution of the detectors. Therefore, a 3 h stability test of the 4H–SiC detector was conducted at a bias voltage of 150 V. A PHS was acquired every 20 min and the variation of energy resolution with time is shown in Fig. 4. It is revealed that the 4H–SiC detector maintained outstanding energy resolutions varying between 2.05 % and 2.43 % throughout the irradiation period. A slow increase of the energy resolution should be due to the polarization effect. As the polarization effect arises from charge accumulation in the bulk volume, a shorter stabilization time is expected at higher charged particle count rate.

In the subsequent neutron experiment, the 4H–SiC detector is used as a thermal neutron counter to detect tritons and α particles with a continuous energy spectrum ranging from 2.73 MeV down to zero [24,27]. The maximum range of these particles in 4H–SiC material is approximately 28 μm, corresponding to 2.73 MeV tritons. At the bias voltage of 150 V, the sensitive region of the 4H–SiC detector is 30 μm, which is sufficient for full charge collection. Based on these test results, the bias voltage of 150 V was chosen for the following neutron experiments.

3. Neutron field experiments in BNCT

The neutron experiments of the 4H–SiC detector were conducted in the neutron field of an AB-BNCT. The neutron spectrum of the field is based on data from Ref. [28], most of the neutrons are in the epithermal region between 0.5 eV and 10 keV. The neutron flux at the beam-exit can be higher than 1×10^9 cm^{-2} s^{-1}. Fig. 5 shows the experiment setup. The 4H–SiC detector was enclosed in a polyethylene moderator center to enhance the sensitivity to epithermal neutrons. The moderator is a cube with a side length of 12 cm and its front face is 180 cm away from the neutron beam-exit surface. A bias voltage of 150 V was applied using a high-voltage supply (ORTEC 556). The detector signals were pre-amplified using a charge amplifier (CIVIDEC C6) and further amplified using a filter amplifier (ORTEC 474). The signals were recorded by the DT5751 digitizer for subsequent analysis.

Fig. 5. Experimental setup of the 4H–SiC detector in an AB-BNCT neutron field.

3.1. Response of the 4H–SiC neutron detector

Here, the C6 amplifier replaced the previously used Cx-L amplifier in the α source measurement due to its fast response. The typical signal of an α particle or low-energy Triton is shown in Fig. 6(a), with the FWHM of ~25 ns. Fig. 6(b) shows the PHS accumulated over the 90 s of the stabilization period of the accelerator with 10 mA proton beam intensity. A distinct peak and continuous distribution are observed at around 1700 channel and between 400 and 1100 channels, respectively. In order to interpret the PHS contributions, the energy distributions of tritons and α particles arriving at the SiC surface were calculated and then fitted to the PHS with Gaussian broadening to reconstruct the PHS, as shown in Fig. 7. The tritons and α particles produced in the convertor respectively have the primary energies of 2.73 MeV and 2.05 MeV. Before being detected by the SiC crystal, they have to undergo energy loss in the convertor. The 2.73 MeV tritons have the range of 33.9 μm in the LiF convertor which is much larger than the convertor thickness of 5 μm. Therefore, the tritons will only lose a slight energy before being detected by the SiC crystal and contributes an obvious peak in the PHS [24,27].

As seen in Fig. 7, the low energy tail of the tritons is ascribed to the tritons incident at steep angles on the SiC surface, as the longer travel distance in the convertor leads to more energy loss. For the 2.05 MeV α particles, they have the range in the convertor of 5.6 μm which is close to the convertor thickness and will lose a lot of energy, resulting in a flat energy distribution. Therefore, the continuous distribution in the PHS is contributed by α particles and the low energy tail of tritons.

The distinct peak of tritons is isolated in the PHS and far away from the background contributions, indicating a good γ background rejection capability of the 4H–SiC detector used as a thermal neutron counter. Based on the reconstructed PHS in Fig. 7, the energy threshold for tritons is determined to be 1.54 MeV, corresponding to approximately the

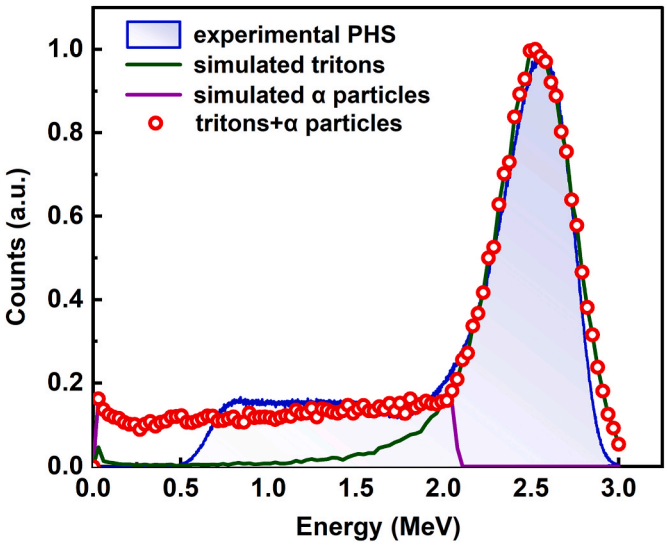

Fig. 7. Simulated pulse height spectrum with Gaussian broadening fitted to the measurement result.

950th channel. Therefore, a suitable threshold can be set at this position to effectively count most tritons and a small portion of α particles for obtaining the responses to exposed neutron fields.

3.2. Linear response of the 4H–SiC neutron detector

Fig. 8(a) shows the correlation between the SiC detector count rate and the neutron yield reflected by the beam current. There are two runs

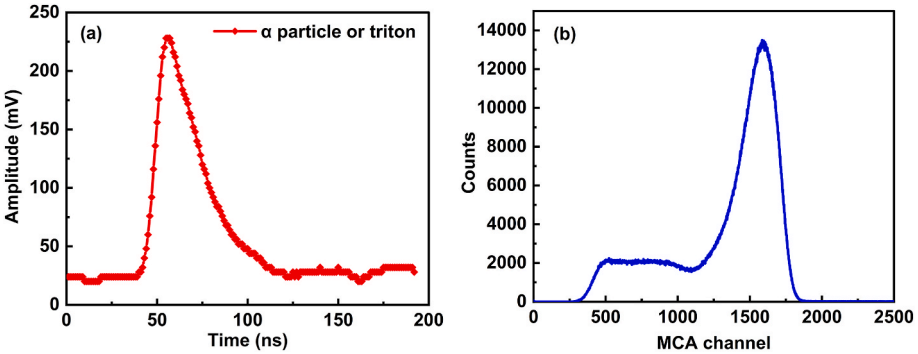

Fig. 6. (a) Output signal of the 4H–SiC detector with a FWHM of ~25 ns under 150 V bias voltage; (b) measured pulse height spectrum.

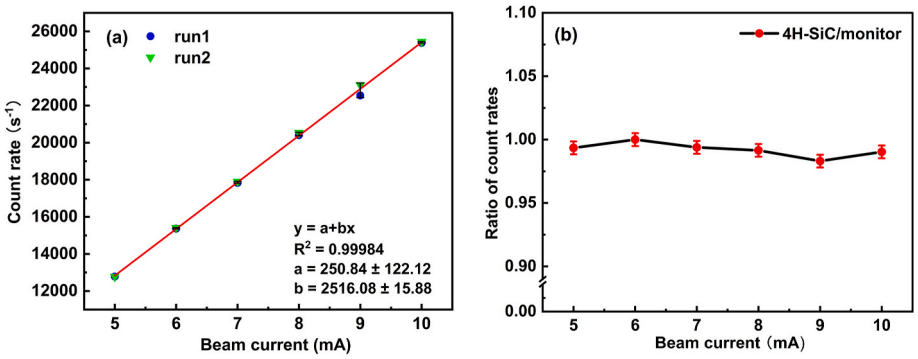

Fig. 8. (a) Correlation between count rates of the 4H–SiC detector and beam currents of the accelerator. Error bars are smaller than the symbol size. (b) Normalized ratio between count rates of a neutron yield monitor of AB-BNCT and 4H–SiC detector.

of measurements. In the first run, the accelerator beam current was ramped up from 5 mA to 10 mA in 1 mA increments. At each beam current, the accelerator was operated for about 3 min, after 90 s the neutron yield was stable and used for data analysis. In the second run, the beam current was adjusted downward to 5 mA under analogous operational conditions. It can be seen that there is a strong correlation between two sets of data (linear correlation coefficient $R^2 = 0.99984$), and no obvious difference between the two runs was found. The normalized ratio between the count rates of the neutron yield monitor and the 4H–SiC detector is also given in Fig. 8(b) for comparison.

The correlation between the count rates of the 4H–SiC detector and the beam currents is comparable to that of the neutron yield monitor, demonstrating that the 4H–SiC detector has a good dynamic range in neutron yield measurement. This feature is mainly ascribed to the fast response of the 4H–SiC detector. The typical drifting time of carriers is far less than 10 ns for the 4H–SiC detector with a sensitive layer of 30 μm [14]. When using the fast charge amplifier C6, the pulse width of the detector is about 25 ns, reflecting a high count rate of up to 4×10^5 s^{-1} with only 1 % count loss. In this test, the maximum count rate is about 2.3×10^4 s^{-1}, far less than the allowed value. It means that even moving closer to the beam exit of AB-BNCT, good linear result can still be obtained.

3.3. Response stability of the 4H–SiC neutron detector

The inevitable polarization effect in 4H–SiC detectors is caused by the long-term trapping of charge carriers by defects in the material. The traps gradually fill over time, leading to the accumulation of space charge, which in turn changes the electric field distribution inside the detector and deteriorates the CCE and signal output [29].

During the irradiation at a beam current of 10 mA, the 4H–SiC detector exhibited an average count rate of 25546.44 s^{-1}, with a relative standard uncertainty of 0.8 % and a maximum deviation of 7.45 % over the 600 s stable period. In Fig. 9(a), the PHSs accumulated over 10s during the initial and final phases of the stable period are also compared and no shape difference is found. The sustained stability of both the count rate and PHS shape demonstrates that polarization effects did not occur in the 4H–SiC detector over the entire 600 s period. During this period, the accumulated counts of the 4H–SiC detector are 1.53×10^7, and the corresponding fluence of charged particles is 1.53×10^5 mm^{-2}. This fluence is 200 higher than the 7.0×10^3 mm^{-2} α particles, beyond which the polarization effect-induced rapid decrease in count rate has been documented in a diamond detector [30]. This comparison revealed the good quality of the 4H–SiC detector used in this work.

Fig. 9(b) presents the time trace of the normalized count rate ratio between the 4H–SiC detector and the standard monitor, with the relative standard uncertainty of 0.955 %, demonstrating a good consistency. The 4H–SiC detector provides a quick response to variations in the neutron fluence rate with a minimum counting period of 0.1 s. It demonstrates the stable operation of the 4H–SiC neutron detectors in neutron field measurements, highlighting their potential advantages for clinical BNCT neutron detection applications.

The technology computer-aided design (TCAD) simulation method was used to evaluate the neutron radiation induced CCE variations, electric field distribution in the sensitive region, and transient current pulse response as a function of neutron fluence at a bias voltage of 150 V [14]. The ratio of 1 MeV equivalent neutron fluence to the neutron fluence in AB-BNCT is determined to be 1.9×10^{-2}. In this simulation, the data for the displacement damage function and the neutron spectrum at a beam exit of an AB-BNCT are obtained from these references [28,31]. The simulation results are shown in Fig. 10. The 4H–SiC detector exhibits high resistance to neutron radiation in BNCT, as shown in Fig. 10(b), with CCEs exceeding 95 % even at neutron fluences up to 10^{16} cm^{-2}. As the neutron fluence is beyond 10^{16} cm^{-2}, the CCE of the

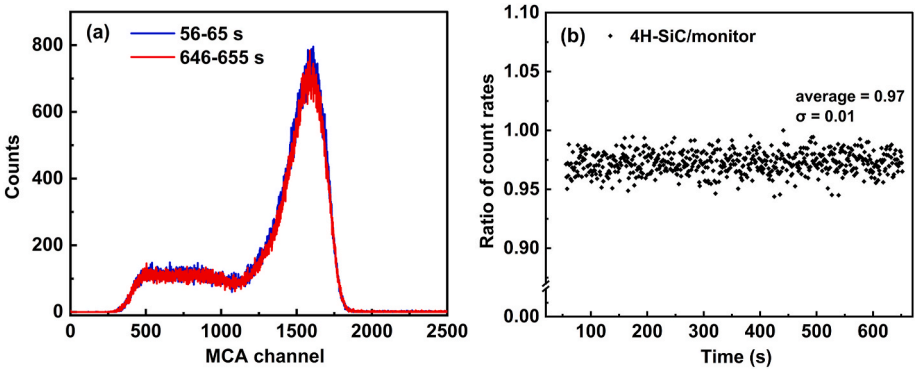

Fig. 9. (a) PHSs accumulated over 10 s during the initial (56–65 s) and final (646–655 s) phases of the stable period; (b) normalized data of the ratio of count rates between the 4H–SiC detector and the standard monitor.

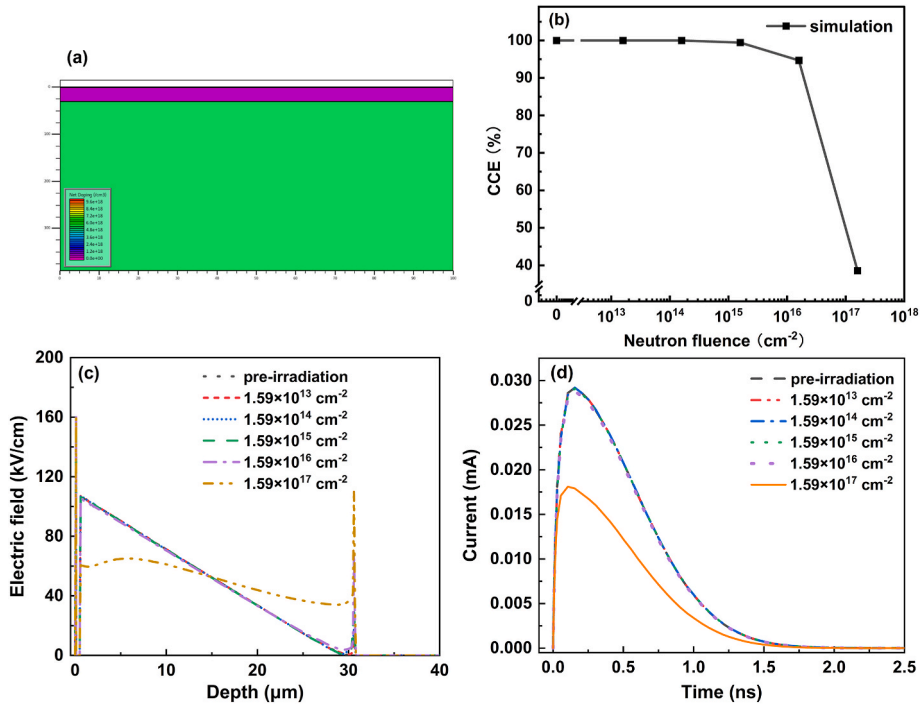

Fig. 10. (a) TCAD model of the 4H–SiC detector; (b) charge collection efficiency of the 4H–SiC detector after neutron irradiation under a 150 V bias voltage; (c) electric field distribution in the sensitive region; (d) transient current pulse response.

detector gradually decreases. It indicates that the 4H–SiC detector should have not obvious CCE degradation for working 10^7 s even when putting the detector at the beam exit position (neutron flux ~10^9 cm^{-2} s^{-1}).

Shown in Fig. 10(c) and (d) are the electric field distributions and transient current pulse response in the sensitive region of the SiC crystal after being irradiated with different neutron fluences. As the neutron fluence gradually increases, neutron irradiation introduces defects into the SiC detector, which act as traps and recombination centers [14]. With increasing fluence, these defects have a possibility to capture charge carriers which will reduce the life time of carriers and create an internal electric field. Finally, deteriorations are observed in the electric field within the sensitive region and the transient current pulses, along with a reduction in the CCE.

4. Conclusion

In this paper the performance of a 4H–SiC detector-based thermal neutron counter was systematically investigated in detail in an AB-BNCT neutron field. Experimental results show that the 4H–SiC detector exhibits a high energy resolution of 2.05 %–5.48 MeV α particles. In AB-BNCT neutron field experiments, the count rate has a strong linear correlation with proton beam intensity (R^2 = 0.9998), indicating excellent neutron linear response characteristics. During stability tests, the detector maintains a stable count rate, with the relative standard uncertainty of only 0.955 % compared to the standard monitor, demonstrating outstanding radiation resistance. The exceptional linear response and radiation resistance stability of the 4H–SiC detector in AB-BNCT neutron field highlight its potential for neutron beam monitoring as a thermal neutron counter. Future research will focus on designing high spatial resolution neutron flux monitors or high energy resolution neutron spectrometers using 4H–SiC detectors for precisely and efficiently AB-BNCT neutron beam monitoring, providing reliable technical support for clinical treatment.

CRediT authorship contribution statement

Qiuying Li: Writing – original draft, Visualization, Software, Methodology, Investigation, Data curation. **Jinlin Song:** Writing – original draft, Visualization, Validation, Software, Methodology, Investigation, Data curation. **Zhimeng Hu:** Writing – review & editing, Validation, Supervision, Resources, Project administration, Methodology, Investigation, Funding acquisition, Conceptualization. **Wenbo Liu:** Visualization, Software, Data curation. **Fule Li:** Visualization, Software, Data curation. **Mingcai Zhong:** Visualization, Software, Data curation. **Pin Gong:** Resources. **Wei Jiang:** Methodology, Investigation, Data curation. **Kang Sun:** Methodology, Investigation, Data curation. **Giuseppe Gorini:** Software, Methodology. **Gabriele Croci:** Software, Methodology. **Meng Li:** Data curation, resources. **Youqun Lai:** Data curation, resources. **Xiaobin Tang:** Writing – review & editing, Supervision, Resources.

Declaration of competing interest

The authors declare that they have no known competing financial interests or personal relationships that could have appeared to influence the work reported in this paper.

Acknowledgments

This work was supported in part by the National Natural Science Foundation of China under Grants 12375297 and 12105144, in part by the International Research Cooperation Project of Jiangsu Province under Grant BZ2024018, in part by the Science and Technology on Metrology and Calibration Laboratory under Grants JLKG2024001C001 and JLKG2023001C001, in part by the Foundation of Graduate Innovation Center in NUAA Grant No. Xcxjh 20230623.

Data availability

Data will be made available on request.

References

[1] A. Mansoor, A. Diego, A. Saverio, et al., in: Advances in Boron Neutron Capture Therapy, International Atomic Energy Agency, 2023.

[2] M. Suzuki, Boron neutron capture therapy (BNCT): a unique role in radiotherapy with a view to entering the accelerator-based BNCT era, Int. J. Clin. Oncol. 25 (2023) 43–50.

[3] R.L. Moss, Critical review, with an optimistic outlook, on boron neutron capture therapy (BNCT), Appl. Radiat. Isot. 88 (2014) 2–11.

[4] M.E. Capoulat, D. Cartelli, M. Baldo, et al., Accelerator-based neutron sources for BNCT, Health Technol. 14 (2024) 1007–1015.

[5] T.A. Bykov, D.A. Kasatov, I.A. Kolesnikov, et al., A study of the spatial charge effect on 2-MeV proton beam transport in an accelerator-based epithermal neutron source, Tech. Phys. 66 (2021) 98–102.

[6] Y. Wang, W. Tang, X. Xu, et al., The impact of beam extraction position in medical Cyclotrons on the efficiency of Liquid targets, China Medical Devices 12 (2010) 7–9.

[7] S. Nakamura, H. Igaki, H. Okamoto, Dependence of neutrons generated by 7Li(p,n) reaction on Li thickness under free-air condition in accelerator-based boron neutron capture therapy system employing solid-state Li target, Phys. Med. 58 (2019) 121–130.

[8] A. Badrutdinov, T. Bykov, S. Gromilov, et al., In Situ Observations of blistering of a metal irradiated with 2-MeV protons, Metals 12 (2017) 558.

[9] M.D. Napoli, SiC detectors: a review on the use of silicon carbide as radiation detection material, Frontiers in physics 10 (2022) 898833.

[10] C. Zhang, K. Yang, H. Li, et al., Performance of 4H–SiC radiation detector after high flux proton and Fe13+ heavy ion beam irradiation, Journal of Radiation Research and Applied Sciences 17 (2024) 100883.

[11] L. Ren, R. Li, Y. Han, et al., High performance 4H–SiC detectors for superheavy elements study, Nucl. Instrum. Methods Phys. Res. Sect. A Accel. Spectrom. Detect. Assoc. Equip. 1072 (2025) 170181.

[12] L. Liu, A. Liu, S. Bai, et al., Radiation resistance of silicon carbide Schottky diode detectors in D-T fusion neutron detection, Sci. Rep. 7 (2017) 13376.

[13] B. Hong, G.Q. Zhong, L.Q. Hu, et al., Diagnostic of fusion neutrons on EAST tokamak using 4H-SiC detector, IEEE Trans. Nucl. Sci. 69 (2022) 639–644.

[14] Y.B. Sun, Z.M. Hu, H. Zhang, et al., Investigation of the performance degradation of 4H-SiC neutron detectors using MCNP and TCAD, IEEE Sens. J. 24 (2024) 4432–4441.

[15] F.H. Ruddy, L. Ottaviani, A. Lyoussi, et al., Silicon carbide neutron detectors for harsh nuclear environments: a review of the state of the art, IEEE Trans. Nucl. Sci. 69 (2022) 792–803.

[16] K.C. Mandal, T.A. Chowdhury, C. Oner, F.H. Ruddy, Design and response testing of boron-diffused silicon carbide neutron detectors for dosimetry and monitoring applications, in: 16th International Symposium on Reactor Dosimetry, 2018, pp. 353–360.

[17] C.B. Hoshor, T.M. Oakes, E.R. Myers, et al., A portable and wide energy range semiconductor-based neutron spectrometer, Nucl. Instrum. Methods Phys. Res. A 803 (2015) 68–81.

[18] P.B. Ugorowski, J.C. Currie, B. Baramsai, et al., Fast neutron spectroscopy with a volumetrically-sensitive, moderating-type neutron spectrometer in a high-radiation environment, Nucl. Instrum. Methods Phys. Res. A 1039 (2022) 166982.

[19] M. Takada, Y. Abe, S. Nakamura, et al., Spectrometer design of low energy neutrons for boron neutron capture therapy, Nucl. Instrum. Methods Phys. Res. A 1020 (2021) 165848.

[20] Z. Long, X. Xia, W. Jiang, et al., Neutron irradiation and polarization effect of 4H-SiC Schottky detector, Nucl. Instrum. Methods Phys. Res. A 1064 (2024) 169326.

[21] A. Massara, S. Amaducci, L. Cosentino, et al., ^{6}LiF Converters for neutron detection: Production Procedures and detector tests, Instruments 7 (2023) 1.

[22] L. Ren, Y. Han, X. Meng, et al., Effect of NO annealing on radiation detection performance of Ni/SiO2/4H-SiC MOS capacitors, Nucl. Instrum. Methods Phys. Res. Sect. A Accel. Spectrom. Detect. Assoc. Equip. 1070 (2025) 170073.

[23] K.C. Mandal, S.K. Chaudhuri, K.V. Nguyen, Correlation of deep levels with detector performance in 4H-SiC epitaxial Schottky barrier alpha detectors, IEEE Trans. Nucl. Sci. 61 (2014) 2338–2344.

[24] X.F. Xie, X. Yuan, X. Zhang, et al., Application of a single crystal chemical vapor deposition diamond detector for deuteron plasma neutron measurement, Nucl. Instrum. Methods Phys. Res. A 761 (2014) 28–33.

[25] X.D. Meng, Y.C. Han, L. Ren, et al., A novel 4H–SiC thermal neutron detector based on a metal-oxide-semiconductor structure, Nucl. Instrum. Methods Phys. Res. Sect. A Accel. Spectrom. Detect. Assoc. Equip. 1068 (2024) 169683.

[26] R. Wang, Y. Huang, D. Yang, Impurities and defects in 4H silicon carbide, Appl. Phys. Lett. 122 (2023) 18.

[27] Z.M. Hu, L.J. Ge, J.Q. Sun, et al., An active Bonner sphere spectrometer capable of intense neutron field measurement, Appl. Phys. Lett. 114 (2019) 233502.

[28] D.Y. Shu, X.B. Tang, C.R. Geng, et al., Novel method exploration of monitoring neutron beam using Cherenkov photons in BNCT, Radiat. Phys. Chem. 159 (2019) 222–230.

[29] M. Rebai, D. Rigamonti, S. Cancelli, et al., New thick silicon carbide detectors: response to 14 MeV neutrons and comparison with single-crystal diamonds, Nucl. Instrum. Methods Phys. Res. A 946 (2019) 162637.

[30] M. Rebai, A. Fazzi, C. Cazzaniga, et al., Time-stability of a single-crystal diamond detector for fast neutron beam diagnostic under alpha and neutron irradiation, Diam. Relat. Mater. 61 (2016) 1–6.

[31] M.O. Patton, R.D. Harris, R.G. Rohal, et al., Strategies for Radiation Hardness Testing of Power Semiconductor Devices. Report NASA/CR—2005-213807, National Aeronautics and Space Administration, 2005.